## Fractal structure of multipartite entanglement in monitored quantum circuits

Vaibhav Sharma\*

Smalley-Curl Institute, Rice University, Houston,
TX 77005 and Department of Physics and Astronomy, Rice University, Houston, TX 77005

Erich J Mueller<sup>†</sup>
Laboratory of Atomic and Solid State Physics, Cornell University, Ithaca, NY 14853
(Dated: November 13, 2025)

We analyze the distribution of multipartite entanglement in states produced in a one-dimensional random monitored quantum circuit where local Clifford unitaries are interspersed with single-site measurements performed with a probability p. This circuit has a measurement-induced phase transition at  $p=p_c$ , separating a phase in which the entanglement entropy scales with the system size (a volume law state) and one in which it scales with the boundary (an area law state). We calculate the entanglement depth, corresponding to the size of the largest cluster of entangled qubits, finding that it scales as a power law with system size in both the phases. The power law exponent is 1 in the volume law phase ( $p < p_c$ ) and continuously decreases to 0 as  $p \to 1$  in the area law phase. We explain this behavior by studying the spatial distribution of entangled clusters. We find that the largest cluster of entangled qubits in these states has a fractal dimension between 0 and 1 and appears to be self-similar. Away from the critical point, this fractal dimension matches the entanglement depth power law exponent.

Introduction — Monitored quantum circuits with random unitary gates and projective measurements have emerged as powerful tools to understand dynamics of entanglement in noisy quantum many-body systems [1]. By varying the parameters of these monitored circuits, such as the relative probabilities of unitary operations and projective measurements, these circuits can exhibit a variety of many body phases and quantum phase transitions between them [2–13]. An iconic example is the measurement-induced entanglement phase transition from a volume law entangled phase to an area law entangled phase [2–5]. These entanglement phase transitions are characterized by the distinct scalings of the bipartite entanglement entropy with system size. Here we study the spatial distribution of multipartite entanglement in such a monitored random circuit, finding a fractal structure.

While bipartite entanglement entropy can distinguish states based on the amount of entanglement across a partition, it does not tell us anything about the spatial range of entanglement or the full complexity of the entanglement structure of the state. As an example, consider the N-qubit Greenberger-Horne-Zeilinger (GHZ) state on a one-dimensional chain,  $\Psi_{GHZ} = |111\cdots\rangle + |000\cdots\rangle$ . It is an area law state as the bipartite entanglement entropy across any partition is independent of the system size N. Such area law behavior indicates that the state contains a very small amount of entanglement. Nonetheless the GHZ state is an example of genuine N-partite entanglement; every qubit is entangled with every other qubit. The bipartite entanglement entropy is insensitive to this feature, and cannot by itself be used to charac-

terize multipartite entanglement. A similar case can be made for states involved in measurement-induced phase transitions. It is important to understand their entanglement properties, beyond simply the bipartite entanglement entropy.

Some previous works have examined multipartite entanglement in systems exhibiting measurement induced phase transitions using quantum Fisher information [14– 17], tripartite entanglement measures [18, 19] and k-party mutual information [20]. Quantum Fisher information provides a lower bound to the number of parties entangled in a state. While it is a valuable tool, it is strongly affected by the choice of the operator used to compute it [21]. Choosing local operators can often lead to an underestimation of these bounds [22]. Tripartite entanglement was found to show some genuine three-qubit long-range entanglement near the measurement induced phase transition [18] but it does not easily generalize to N-partite entanglement computations. Here we explore multipartite entanglement in such states by calculating the entanglement depth, which corresponds to the size of the largest cluster of entangled qubits. We also study the spatial structure of this cluster. This approach gives us a representation of long-range entanglement in these monitored circuits, which is basis agnostic, in the sense that we do not need to choose a particular operator or system partition. This enables us to quantify how multipartite entanglement is affected by a finite probability of projective measurements in random quantum circuits.

We study circuits where random two-qubit Clifford unitaries are interspersed with single-qubit Pauli measurements. In a given circuit layer, the latter occur with a probability p. This circuit exhibits a measurement-induced entanglement phase transition between the area and volume law phase [3, 4]. By using the formalism developed in [23], we construct a number of metrics of

<sup>\*</sup> vaibhavsharma@rice.edu

 $<sup>^{\</sup>dagger}$  em256@cornell.edu

multipartite entanglement. This procedure allows us to extract the largest non-separable cluster of qubits. The size of that cluster is known as the entanglement depth. We find that the entanglement depth scales as a power law with system size in both the area and the volume law phase. There is long range entanglement that persists even within the area law phase. It is more robust to single qubit projective measurements as compared to the bipartite entanglement entropy. We further find that the largest qubit cluster is well described as a fractal whose fractal dimension tracks the entanglement depth power law exponent away from the entanglement phase transition critical point. This hints towards a self similarity in the largest entangled cluster.

Circuit Model — Figure 1(b) shows our circuit model where a one-dimensional chain of L qubits evolves under random two-qubit Clifford unitaries and single-site projective measurements in a brickwork arrangement [3– 5]. At each odd (even) time step, nearest-neighbor qubits connected by odd (even) bonds are acted upon by a random two-qubit Clifford unitary. Then at each step, every qubit is projectively measured in the z-basis with a probability p. Due to the Gottesman-Knill theorem [24], the states generated by this circuit are stabilizer states which can be efficiently simulated by classical computers despite extensive entanglement. For system size L, the stabilizer formalism keeps track of the quantum state by storing L binary strings of length 2L [13]. We start with a product state in the z-basis and evolve under the random Clifford circuit at a given measurement probability p. We proceed for 4L steps to reach a steady state. Our results are obtained by ensemble averaging over 500 such steady state realizations for system sizes up to L = 240.

Entanglement Structure Calculation — We use the method developed in [23] to extract the entanglement depth and construct the largest cluster of entangled qubits. Our approach involves constructing an entanglement structure diagram which gives a hierarchical representation of how various qubits are entangled with oneanother. It contains information that we do not use here, but nonetheless is an efficient method of constructing the largest cluster of entangled qubits. Here, we briefly recap the strategy. It involves grouping qubits into clusters characterized by a parameter w. Such a w-cluster has the property that each qubit within it has non-zero total correlations with at least (w-1) other qubits in the cluster; the total correlation of w qubits is  $I = \sum_{i=1}^{w} S_i - S_{\text{cluster}}$ . Here  $S_i$  is the entanglement entropy of qubit i with respect to the rest of the system and  $S_{\text{cluster}}$  is the entanglement entropy of the w qubit group with the rest of the system.

This construction is iterative where a cluster found in one iteration becomes an indivisible new element in the subsequent iterations. We can then continue to recursively group these clusters into new clusters until all qubits have been assigned to large decoupled clusters. The overall state can be written as a tensor product state over these decoupled clusters. Each large cluster itself

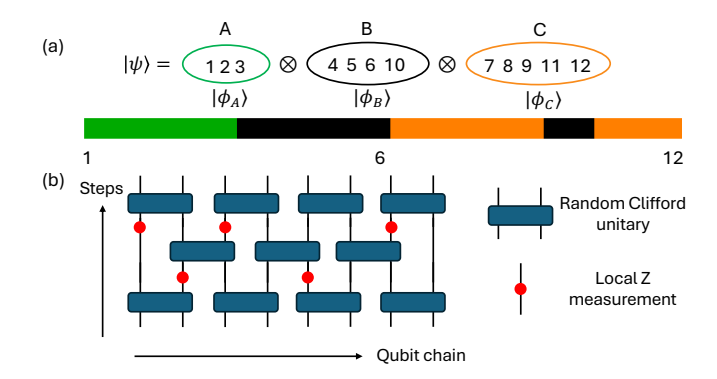


FIG. 1. (a) Entanglement structure schematic of a twelvequbit state  $|\psi\rangle$ . The state is separable into a tensor product over clusters A (green),B (black) and C (orange) denoted as  $|\psi\rangle = |\phi_A\rangle \otimes |\phi_B\rangle \otimes |\phi_C\rangle$ . The colored bar shows the qubits arranged in their native spatial order. The entanglement depth of this state is 5, corresponding to the size of the largest cluster C. (b) Monitored circuit in brickwork form with two-qubit random Clifford unitaries and local projective z-basis measuremements with probability p.

describes a set of qubits that are genuinely multipartite entangled. The size of the largest cluster denotes the entanglement depth of the state.

Fig. 1 shows an abreviated schematic of an entanglement structure of some twelve qubit state,  $|\psi\rangle$ . There are three large decoupled clusters over regions A, B and C suggesting that  $|\psi\rangle = |\phi_A\rangle \otimes |\phi_B\rangle \otimes |\phi_C\rangle$ . Here  $|\phi_A\rangle$ ,  $|\phi_B\rangle$  and  $|\phi_C\rangle$  denote some genuine multipartite entangled states that cannot be further written as tensor product states over smaller subsystems. The entanglement depth of the state in this schematic example is 5 as it corresponds to the size of the largest cluster, denoted by region C.

As a function of system size, this method scales exponentially for unitary-only circuits and polynomially for local measurement-only circuits [23]. The computational time can be further improved by coarse graining the system. For that, instead of considering each qubit individually in the first iteration of the method, we can group a few neighboring qubits together, and then consider these groups as the individual entities in the clustering method.

Entanglement depth and long-range entanglement — We calculate the average entanglement depth of the steady state ensemble generated by the monitored Clifford circuit as a function of the single-site measurement probability p and system size L. A growth in entanglement depth with system size indicates the presence of long-range entanglement. In our analysis, we use a two-qubit coarse graining procedure before evaluating the entanglement structure diagram and extracting the entanglement depth. There are two reasons for using this coarse graining. First, due to the two-qubit unitary gates in our circuit, there are always neighboring pairs of qubits which are entangled, giving a lower bound of 2 on the entanglement depth in the absence of coarse graining.

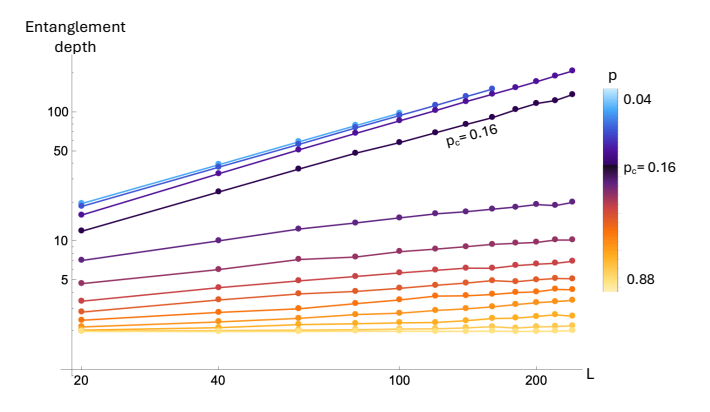


FIG. 2. Log-log plot of average entanglement depth as a function of system size L for the steady state ensemble of states formed by applying random nearest-neighbor two-site clifford gates, interspersed with random single site measurements. The probability of a local measurement is p. The curves are plotted in steps of 0.04 for  $p < p_c$  and in steps of 0.08 for  $p > p_c$ . There is a phase transition at  $p = p_c \sim 0.16$  [3, 4].

A system size dependent population of such neighboring pairs could erroneously be mistaken for a sign of long-range entanglement. Second, coarse graining over pairs of sites leads to shorter computational times and lets us go to higher system sizes when p is sufficiently close to the volume law phase.

Figure 2 shows the entanglement depth as a function of system size, L for various measurement probabilities, p on a log-log plot. We can see that the entanglement depth grows as a power law both within the volume law phase ( $p < p_c = 0.16$ ) and the area law phase where  $p > p_c$ . This scaling captures the presence of long-range entanglement within the area law phase that is not manifest in bipartite entanglement measures. The slope on the log-log plot seems to be nearly constant when  $p \leq p_c$  and reduces as p increases within the area law phase. We note that deep within the volume law phase, we limit ourselves to small L due to the computational difficulty of calculating the entanglement structure for volume law states.

We use a robust linear regression technique called the Thiel-Sen estimator [25, 26] to fit this data to a straight line and extract the power law exponent  $\gamma$  such that  $D \propto L^{\gamma}$ , where D denotes the entanglement depth. In the End Matter, we discuss the Thiel-Sen estimator for regression and how we get error bars for the extracted slopes. The results are shown as blue data points in Fig. 3. We can see that the power law exponent is  $\gamma=1$  within the volume law phase and at the critical point. In the area law phase,  $\gamma$  continuously decreases to 0 as  $p \to 1$ . The plot shows a sharp drop in the power law exponent at the volume law - area law transition at  $p_c=0.16$ . For  $0.3 \lesssim p \lesssim 0.6$ , there appears to be a plateau in  $\gamma$ . There is a knee at  $p \sim 0.6$ . For  $p \gtrsim 0.6$ , the slopes decrease to 0 as we approach p=1 where all qubits are expected to

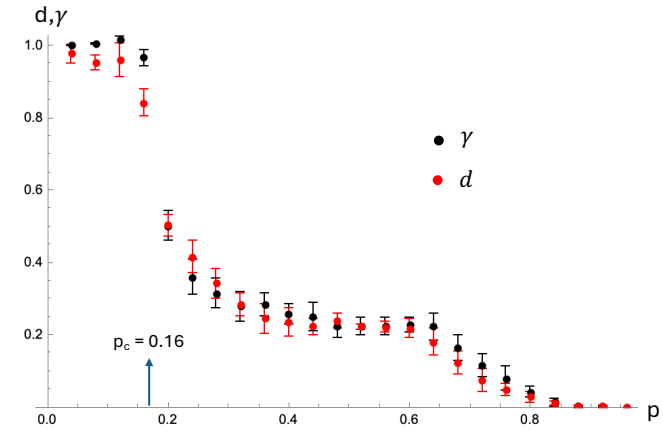


FIG. 3. Power law exponent of entanglement depth growth with system size,  $\gamma$  (blue dots) and fractal dimension, d of the largest cluster of entangled qubits as a function of measurement probability, p. The critical point for the volume law-area law phase transition is shown as  $p_c = 0.16$ .

be disentangled with each other.

The average entanglement depth denotes the ensemble average of the largest cluster size in each realization of the random circuit. In the volume law phase, there is extensive entanglement and the bipartite entanglement entropy itself grows linearly with system size. Thus we expect the largest cluster to also grow linearly with system size, consistent with our observation that  $\gamma=1$  for  $p< p_c$ . At p=0, we expect all qubits to be entangled and the largest cluster exactly spans the entire system. Beyond the volume law phase,  $p>p_c$ , the bipartite entanglement entropy either grows logarithmically with system size (at critical point) or saturates quickly to a constant. However, we find that the largest cluster continues to grow with system size even in these regimes.

The number of entangled spins in the largest cluster grows, despite the saturation in the number of clusters which cross any bipartition. This suggests that there are a small number of very large clusters. Increasing the frequency of measurements, by increasing p, shrinks the size of the largest cluster, but it still grows with L. There is a marked robustness to these states, which is very different from what we saw in the GHZ example. A single measurement on a GHZ state results in a disentangled state.

As noted, Fig. 3 shows a distinct knee near p=0.6. This occurs when the ensemble averaged entanglement depth is of order, D=2. For larger p, the ensemble predominantly contains realizations where D=2. At smaller p, one instead has a broader distribution of D. The location of the knee is sensitive to the degree of course graining that we perform.

**Fractal Structures** — Here we study the spatial structure of the largest entangled cluster. Earlier we showed that the size of this cluster D grows with system size as  $D \sim L^{\gamma}$ , with  $0 < \gamma < 1$  in the area law

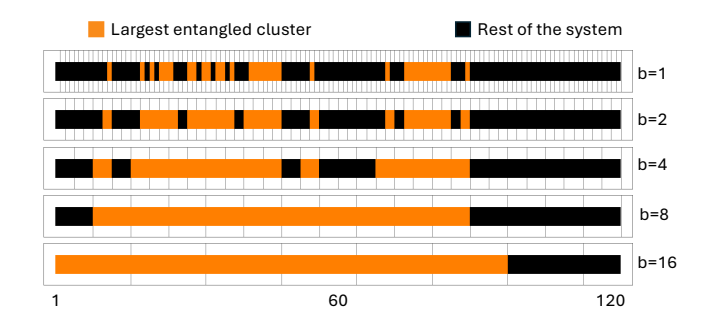


FIG. 4. A typical 120 qubit state generated at measurement probability, p=0.2. The same state is shown with different coarse-graining scales, denoted by gridlines enclosing b qubits. For a given coarse-grained picture, the orange squares denote qubits that are part of the largest entangled cluster while black squares denote the remaining qubits. The orange cluster spans the entire system, but is filled with 'holes' of multiple sizes that break it into discontinuous pieces.

phase. This power law is suggestive of a fractal shape, analogous to a Cantor set.

Figure 4 shows a typical 120-qubit state generated by our monitored circuit model with the measurement probability, p = 0.2. The qubits are arranged in their native spatial order. The orange squares denote qubits which are part of the largest entangled cluster while the black squares denote the rest of the qubits. Without coarsegraining (b = 1), we can see that the largest cluster is not a continuous block but instead contains a number of unentangled qubits which appear as holes in the cluster. These holes span multiple scales, as is illustrated by the coarse-grained clusters characterized by different values of b as shown in Fig. 4. The presence of holes at multiple coarse grained levels implies that the largest cluster of entangled qubits is a fractal object. The observed pattern of holes is analogous to ones seen in mathematical fractals such as the Sierpienski triangle where there are triangle-shaped holes at every coarse-grained level. An even better analogy could be made with random Cantor sets [27]. Regardless, visually the pattern in Fig. 4 is suggestive of a fractal.

We use a box counting method to extract the fractal dimension of the largest cluster. For a given state in our ensemble, we first coarse-grain by grouping b neighboring qubits into indivisible boxes. We then extract the entanglement structure diagram to get the coarse-grained entanglement depth. The detailed procedure is explained in the End Matter. We count the number of boxes,  $N_b$  that are required to tile the largest entangled cluster (such as the orange region in Fig. 4). The fractal dimension, d is then defined as,  $d = -\ln N_b/\ln b$ .

We use box sizes ranging from 2 to 20 and calculate the ensemble-averaged value  $N_b$  for different measurement probabilities p. We used a system size L=240 for  $p\geq 0.12$  and the results are shown in a log-log plot in Fig. 5. We can see that the log-log plots show a linear relationship between  $\ln N_b$  and  $\ln b$  with a negative

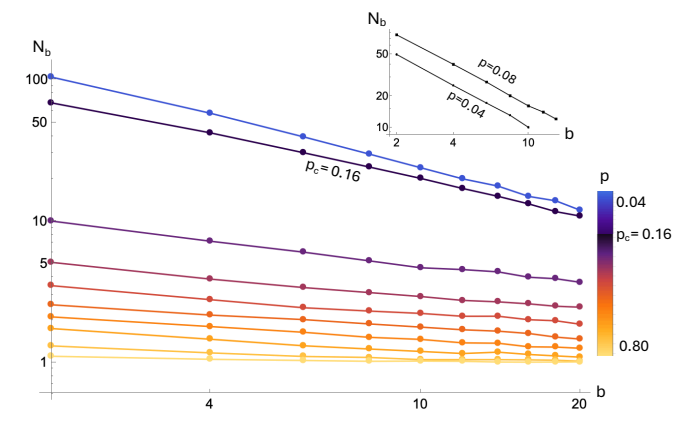


FIG. 5. Log-log plot of number of boxes,  $N_b$  as a function of box size, b for various measurement probabilities, p. The curves are plotted in steps of 0.04 for  $p < p_c$  and in steps of 0.08 for  $p > p_c$ . The inset separately shows the same data deep in the volume law phase for p = 0.04, p = 0.08.

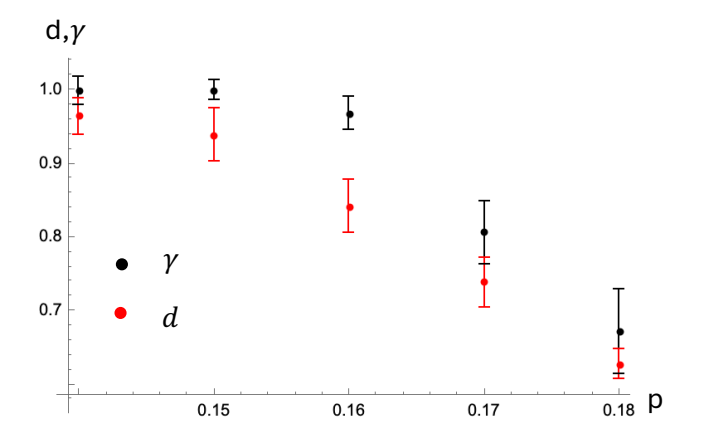


FIG. 6. Power law exponent of entanglement depth growth with system size,  $\gamma$  (blue dots) and fractal dimension, d of the largest cluster of entangled qubits as a function of measurement probability, p near the entanglement phase transition critical point,  $p_c = 0.16$ .

slope, suggesting a fractal structure. The magnitude of the slope of the curve gives the fractal dimension. We again used the Thiel-Sen estimator to extract the fractal dimension from these data. Deep within the volume law phase, we use smaller system sizes (L=100,160 for p=0.04,0.08 respectively) to extract the fractal dimension.

The results are shown as yellow data points in Fig. 3. We can see that the largest entangled clusters are fractal objects with a fractal dimension between 0 and 1. In the area law phase, the fractal dimension agrees with the entanglement depth exponent up to the error bars which are inferred from the accuracy of the power law fit. At the critical point (p=0.16), there is however a small, but statistically significant, difference between the two. Fig. 6 shows the region close to the critical point and we see that the fractal dimension and entanglement

depth power law exponent extracted from our fits do not agree close to the critical point. This discrepancy reduces as we go away from the critical point deeper into the volume law phase. These discrepancies may be related to logarithmic corrections to scaling, finite size effects, or some other additional structure which emerges at the critical point.

The fractal structure that emerges in this system is a consequence of the competition between the nearest neighbor unitary operations in our circuit, and the local measurements. A unitary operation between a qubit in the largest cluster, and one outside of the cluster, will typically cause it to grow. Conversely, measuring a qubit which is within the largest cluster will cause it to shrink. It is, however, nontrivial to deduce the amount by which the cluster grows/shrinks. For example, a single unitary operation may combine two clusters. Measuring a single qubit may simply remove it from the cluster, or, as is demonstrated by the GHZ state, it could cause the entire cluster to dissolve. Evidently, in steady state, the qubits are entangled in a heirarchical manner, where there are structures on multiple scales. Such emergent fractal hierarchies are familiar from models such as percolation [28]. Here we appear to be able to continuously tune the fractal dimension by varying the parameter p.

We emphasize that the fractals we see here are approximate physical fractals and not exact mathematical fractals. An exact mathematical fractal would show the same structure at arbitrarily small and large scales. In our case, the smallest physical scale we have is a single qubit. Our finite system size limits the largest possible scale. Thus, for system size L=240, our box sizes can cover only a few powers of 2 ranging from b=2 to b=20. In this intermediate size regime, the ensemble averaged largest cluster of entangled qubits is well described as a fractal object. While we believe that this behavior will extend to the thermodynamic limit, it is possible that we are observing a finite size effect which would not be present in numerical experiments on larger systems.

**Summary and Outlook** — Given that monitored circuits exhibit entanglement phase transitions, it is natural to ask about the resulting structure of multipartite

entanglement. In this work, we use the method developed in [23] to calculate the entanglement depth of the ensemble of states generated by random Clifford circuits where random two-qubit unitary gates are interspersed with single qubit projective measurements with probability p.

We find that significant multipartite entanglement survives even within the area law phase. Across both the volume and area law phases, we find that the entanglement depth scales as a power law with system size, demonstrating that long-range entanglement and multipartite entanglement are more robust to measurements than bipartite entanglement entropy. We also analyze the fractal dimension of the largest cluster of entangled qubits as a function of p using a box counting method and find that it is well described as a fractal with a fractal dimension between 0 and 1. The fractal dimension coincides with the entanglement depth scaling exponent in both the volume law and area law phase away from the critical point. At the critical point, the depth exponent that we extract is somewhat higher than the fractal dimension.

Multipartite entanglement measures offer a fresh perspective to analyze the properties of states produced in random quantum circuits. They are able to better reveal the presence of long-range entanglement structures which are invisible to other measures such as bipartite entanglement entropy and mutual information. Entanglement depth is one such multipartite entanglement metric. Unlike other metrics, such as Quantum Fisher information, it is operator-independent. Using the techniques in [23], the entanglement depth can be efficiently extracted for many classes of stabilizer states. It would be interesting to explore other random circuit models exhibiting quantum criticality using this multipartite entanglement perspective and analyze analogous structures within non-stabilizer states.

Acknowledgements — VS acknowledges support from the J. Evans Attwell Welch fellowship by the Rice Smalley-Curl Institute. EJM acknowledges support from the National Science Foundation under Grant No. PHY-2409403.

M. P. Fisher, V. Khemani, A. Nahum, and S. Vijay, Random quantum circuits, Annual Review of Condensed Matter Physics 14, 335 (2023).

<sup>[2]</sup> S. Choi, Y. Bao, X.-L. Qi, and E. Altman, Quantum error correction in scrambling dynamics and measurementinduced phase transition, Phys. Rev. Lett. 125, 030505 (2020).

<sup>[3]</sup> Y. Li, X. Chen, and M. P. A. Fisher, Quantum zeno effect and the many-body entanglement transition, Phys. Rev. B 98, 205136 (2018).

<sup>[4]</sup> Y. Li, X. Chen, and M. P. A. Fisher, Measurement-driven entanglement transition in hybrid quantum circuits, Phys. Rev. B 100, 134306 (2019).

<sup>[5]</sup> B. Skinner, J. Ruhman, and A. Nahum, Measurementinduced phase transitions in the dynamics of entanglement, Phys. Rev. X 9, 031009 (2019).

<sup>[6]</sup> M. Ippoliti, M. J. Gullans, S. Gopalakrishnan, D. A. Huse, and V. Khemani, Entanglement phase transitions in measurement-only dynamics, Phys. Rev. X 11, 011030 (2021).

<sup>[7]</sup> A. Lavasani, Y. Alavirad, and M. Barkeshli, Measurement-induced topological entanglement transitions in symmetric random quantum circuits, Nature Physics 17, 342 (2021).

<sup>[8]</sup> C.-M. Jian, Y.-Z. You, R. Vasseur, and A. W. W. Ludwig, Measurement-induced criticality in random quantum cir-

- cuits, Phys. Rev. B **101**, 104302 (2020), arXiv:1908.08051 [cond-mat.stat-mech].
- [9] S. Sang and T. H. Hsieh, Measurement-protected quantum phases, Phys. Rev. Research 3, 023200 (2021).
- [10] X. Turkeshi, R. Fazio, and M. Dalmonte, Measurement-induced criticality in (2+1)-dimensional hybrid quantum circuits, Phys. Rev. B 102, 014315 (2020).
- [11] P. Sierant, M. Schirò, M. Lewenstein, and X. Turkeshi, Measurement-induced phase transitions in (d +1) dimensional stabilizer circuits, Phys. Rev. B 106, 214316 (2022), arXiv:2210.11957 [cond-mat.stat-mech].
- [12] A. Lavasani, Z.-X. Luo, and S. Vijay, Monitored quantum dynamics and the kitaev spin liquid, Phys. Rev. B 108, 115135 (2023).
- [13] V. Sharma, C.-M. Jian, and E. J. Mueller, Subsystem symmetry, spin-glass order, and criticality from random measurements in a two-dimensional bacon-shor circuit, Phys. Rev. B 108, 024205 (2023).
- [14] A. Lira-Solanilla, X. Turkeshi, and S. Pappalardi, Multipartite entanglement structure of monitored quantum circuits, Phys. Rev. Lett. 135, 080401 (2025).
- [15] A. Paviglianiti and A. Silva, Multipartite entanglement in the measurement-induced phase transition of the quantum ising chain, Phys. Rev. B 108, 184302 (2023).
- [16] G. Di Fresco, B. Spagnolo, D. Valenti, and A. Carollo, Metrology and multipartite entanglement in measurement-induced phase transition, Quantum 8, 1326 (2024).
- [17] P. M. Poggi and M. H. Muñoz-Arias, Measurementinduced multipartite-entanglement regimes in collective spin systems, Quantum 8, 1229 (2024).
- [18] S. J. Avakian, T. Pereg-Barnea, and W. Witczak-Krempa, Long-range multipartite entanglement near measurement-induced transitions, Phys. Rev. Res. 7, 023135 (2025).
- [19] G. Xu and Y.-X. Zhang, Multipartite greenberger-hornezeilinger entanglement in monitored random clifford circuits (2024).
- [20] J. Allen and W. Witczak-Krempa, Spatial structure of multipartite entanglement at measurement induced phase transitions (2025), arXiv:2509.12109 [quant-ph].
- [21] P. Hyllus, W. Laskowski, R. Krischek, C. Schwemmer, W. Wieczorek, H. Weinfurter, L. Pezzé, and A. Smerzi, Fisher information and multiparticle entanglement, Phys. Rev. A 85, 022321 (2012).
- [22] Y. Wang, Y. Fang, F. Xie, and Q. Si, Local and non-local entanglement witnesses of fermi liquid (2025), arXiv:2502.13958 [cond-mat.str-el].
- [23] V. Sharma and E. J. Mueller, Multipartite entanglement structures in quantum stabilizer states, Phys. Rev. A 112, 012411 (2025).
- [24] S. Aaronson and D. Gottesman, Improved simulation of stabilizer circuits, Phys. Rev. A 70, 052328 (2004).
- [25] H. Theil, A rank-invariant method of linear and polynomial regression analysis, in *Henri Theil's Contributions to Economics and Econometrics* (Springer Netherlands, 1992) p. 345–381.
- [26] P. K. Sen, Estimates of the regression coefficient based on kendall's tau, Journal of the American Statistical Association 63, 1379–1389 (1968).
- [27] R. R. Tremblay and A. P. Siebesma, Void distribution of random cantor sets, Phys. Rev. A 40, 5377 (1989).
- [28] J. T. Chayes, L. Chayes, and R. Durrett, Connectivity properties of mandelbrot's percolation process, Probabil-

- ity Theory and Related Fields 77, 307-324 (1988).
- [29] C. Leys, C. Ley, O. Klein, P. Bernard, and L. Licata, Detecting outliers: Do not use standard deviation around the mean, use absolute deviation around the median, Journal of Experimental Social Psychology 49, 764–766 (2013).
- [30] M. G. Akritas, S. A. Murphy, and M. P. Lavalley, The theil-sen estimator with doubly censored data and applications to astronomy, Journal of the American Statistical Association 90, 170–177 (1995).

## I. END MATTER

## A. Thiel-Sen Linear Regression

Here we briefly describe the Thiel-Sen regression method we used to extract the slope and the error bars corresponding to the straight line fits of the entanglement depth and box-counting data in the log scale in Fig. 2 and Fig. 5. Given a set of data points  $\{y_i, x_i\}$ , we first calculate the slopes  $m_{i,j} = (y_j - y_i)/(x_j - x_i)$  obtained from all possible pairs of data points. Only pairs with distinct values of  $x_i$  and  $x_j$  are considered. Here i and j are indices identifying the data points.

The median, m of the data set  $m_{i,j}$  is the Thiel-Sen estimator of the slope for the straight line fit. The error in the estimated slope is given by the median absolute deviation of this data set. It is obtained by calculating the median of the data set,  $\{|m-m_{i,j}|\}$ . This quantity is also a measure of statistical dispersion, analogous to the standard deviation that averages the squared distance from the mean of a data set. For normal distributions, the median absolute deviation and standard deviation are proportional [29].

In contrast to the least-squares method, the Thiel-Sen method is insensitive to outliers and works well for noisy data that is not normally distributed, making it a more robust linear regression method [30]. For the data here, however, the two approaches give similar results.

## B. Box Counting Method

Here we describe the box counting method we used to extract the fractal dimension of the largest entangled cluster. For a given state generated by our random circuit, we first coarse-grain our system by grouping b neighboring qubits together. With qubits labeled by numbers corresponding to their native spatial order, we group qubits labeled from 1 to b, then from b+1 to 2b and so on for a system size L, giving us  $\lceil L/b \rceil$  boxes. These boxes are considered as indivisible entities, coarse-graining any entanglement structure that we obtain.

We then compute the coarse-grained entanglement structure using the method in [23]. The resulting structure for different coarse-graining scales b shown in Fig. 4 where the gridlines show the box sizes visually. We count

the number of boxes involved in the largest cluster within this entanglement structure and term it as  $N_b$ . We repeat

the calculation with different box sizes b, extracting  $N_b$  as a function of b from each of the entanglement structures.